IOP Publishing Smart Materials and Structures
Smart Mater. Struct. **26** (2017) 035067 (11pp) https://doi.org/10.1088/1361-665X/aa5fe5

Magnetic field dependent electric conductivity of the magnetorheological fluids: the influence of oscillatory shear

Xiaohui Ruan, Yu Wang, Shouhu Xuan[1] and Xinglong Gong[1]

CAS Key Laboratory of Mechanical Behavior and Design of Materials, Department of Modern Mechanics, University of Science and Technology of China, Hefei 230027, People's Republic of China

E-mail: xuansh@ustc.edu.cn and gongxl@ustc.edu.cn

Received 28 October 2016, revised 7 February 2017
Accepted for publication 10 February 2017
Published 23 February 2017

Abstract

In this work, the influence of oscillatory shear on the magnetic field dependent electric conductivity of the magnetorheological fluid (MRF) was reported. Upon applying a 0.96 T magnetic field, the electric conductivity could increase about 1500 times larger than the one without magnetic field. By increasing the volume fraction of carbonyl iron particles in the MRF from 5% to 30%, the electric conductivity increased about 565 times. Under applying an oscillatory shear, the resistance of the MRF decreased and it oscillated synchronously with the oscillatory shear. Interestingly, the larger shear strain led to larger oscillatory amplitude of the resistance. A particle–particle resistance model and a semi-empirical formula were proposed to investigate the influence of the oscillatory shear on the electric conductivity. The fitting results matched the experimental results very well. At last, a possible mechanism was proposed to explain the changes of resistance.

Keywords: electric conductivity, magnetic field, oscillatory shear, particle–particle resistance model, semi-empirical formula

(Some figures may appear in colour only in the online journal)

1. Introduction

Magnetorheological fluids (MRFs), which were usually obtained by dispersing micrometer size magnetic particles in liquid phase [1–3], had been widely researched because of their excellent mechanical properties. When a magnetic field was applied, the magnetic particles inside MRFs arranged into chains or columnar structures, thus the viscosity would greatly change [4–8]. MRFs could return to the original state just when the magnetic field was removed. Due to the controllable and reversible rheological properties, many magnetorheological (MR) equipments, such as MR damper [9, 10] and MR brake [11, 12] had been developed. These devices had been broadly used in automobile suspensions systems [13–17], bridge-stay cables [18–20], and medical apparatus/instruments [21, 22]. Thanks to the continuous efforts by various groups, the significant success had been achieved in studying the rheological properties and the MR mechanism.

Because the columnar or chain-like structures inside the MR materials were composed of conductive carbonyl iron particles (CIPs), the MR materials could transform from insulator to conductor by varying the external stimuli, such as magnetic field, mechanical pressure, and temperature [23, 24]. This unique tunable conductivity enabled the MR materials to be widely applied in electric capacitors, transformation sensors, force sensors, magnetic sensors and so on [25–27]. Many interesting works had been done to study the electrical conductive of MR materials. Martin *et al* reported a high conductive composite by dispersing gold-coated magnetic particles in a polymeric resin. The conductivity of the composites was extremely sensitive to the compression, so these composites could be useful as sensor materials [28]. Bica *et al* had researched the influence of magnetic field and compression pressure on the electrical conductivity of MR elastomers

[1] Authors to whom any correspondence should be addressed.

Table 1. Compositions of MRF samples.

Samples	MRF-5	MRF-10	MRF-15	MRF-20	MRF-25	MRF-30
CIPs (g)	36	72	108	144	180	216
Silicone oil (ml)	93	88	83	78	73	68
Stearic acid (g)	0.72	1.44	2.16	2.88	3.60	4.32

[25, 26]. Pang *et al* improved the electrical conductivity of MR plastomers by doping graphite particles. The experimental results showed that the resistance of non-doped MR plastomers was approximately 10 000 times higher than the resistance of graphite doped MR plastomers [29].

The conductive mechanism was very important for their practical application. Kchit and Bossis *et al* performed a systematic study on the conductive mechanism of MR elastomers and they presented that the resistance of MR elastomers mainly came from the interface. Therefore, the roughness parameter, the thickness of the oxide layer and the thickness of the polymer layer also influenced the conductivity of the materials [30]. By investigating the stimuli dependent impedance of conductive MR elastomers [31], Wand *et al* defined a coefficient R_d to characterize the damage of the microstructure. Xu *et al* proposed an equivalent circuit model to study the electric conductivity of MR plastomers, which revealed that the rearrangement of particles induced by a magnetic field changed the thickness of the interface layer of electrode-MR plastomers thus dramatically influenced the conductivity of MR plastomers [32].

Though chain or columnar structures were formed when the magnetic field was applied, the insulating layer between the nearby particles had a negative influence on the conductivity of the MR materials. Doping some conductivity additives into the traditional MR materials was the common method to improve the conductivity of the MR materials [33–35]. Li *et al* found that the mechanical and conductive properties were both improved by doping graphite into MR elastomers [36, 37]. By connecting the neighboring parallel chains and connecting the disconnected iron chains, the graphite contributed to improving the conductivity of MR elastomers. Some other additives, such as silvers, graphene and carbon nanotubes [38] or some other matrices like ionic liquids and ion gels [39–41], were used to improve the conductivity of MR materials [42].

Most of the previous researches were mainly focused on MR elastomers and MR plastomers, however, the electrical conductivity of MRFs has not been insensitively studied. Since the dynamic characteristic of the CIPs columns in the MRFs, the previous static or quasi-static analysis could not illustrate the conductive property of the MRFs exactly. In this work, the conductivity of MRFs under dynamic state was systematically investigated. Here, the influence of oscillatory shear on the magnetically dependent electrical conductive properties of MRFs was conducted. It was found that the resistance of MRFs decreased sharply with increasing of the CIP volume fraction and magnetic field. When an oscillatory shear was applied, the resistance oscillated synchronously with the oscillatory shear. Finally, a particle–particle resistance model was developed and a semi-empirical formula was proposed to investigate the mechanism of the magnetic field dependent conductivity.

2. Experimental

2.1. Sample preparation

The materials used for the preparation of MRFs were carbonyl iron particles (CIPs, CN, BASF, Germany, the average particle size was about 6 μm), silicone oil (Sigma, the viscosity is 10 mPa s), stearic acid (Sinopharm Chemical Reagent Co. Ltd, China).

MRF samples with different CIPs volume fraction were prepared by the following method. Firstly, the CIPs and stearic acid were dispersed into the silicone oil and the mixture was homogenized by using a mechanical stirrer. Then, the mixture was transferred to an hot oven and the temperature of the oven was maintained at 100 °C until the stearic acid was dissolved completely. Then, the mixture was carefully taken out and stirred until it was cooled to room temperature. After that, the mixture was ball-milled for 24 h by a Planetary Muller. At last, MRFs were transferred to a vial for the subsequent testing. In our experiment, six samples with the CIPs volume fraction varied from 5% to 10%, 15%, 20%, 25%, 30% were prepared. For simplicity, they were named as MRF-5, MRF-10, MRF-15, MRF-20, MRF-25, MRF-30, respectively. The compositions of the six samples were shown in table 1.

2.2. Experimental system

Figure 1 showed the schematic of the experimental system used to characterize the conductivity of the MRFs. The system consisted of three parts: a commercial rheometer Physica MCR301 (Anton Paar, Austria) equipped with an electrical magnetic accessory MRD180, a Modulab material test system (MTS, Solartron analytical, AMETEK advanced measurement technology, Inc., United Kingdom) and a data storage and analyzing system. The MRF sample was located between two aluminum foil electrodes. The two electrodes were fixed on the rotor and substratum of the rheometer by insulating tape. The rheometer could supply a uniform magnetic field from 0 to 0.96 T. An oscillatory shear with different frequency and strain could also be supplied by the rheometer. The modulab MTS could supply a direct voltage excitation and measure the responsive current. Finally, all the data would be saved in the data storage and analyzing system.

In our experiment, the distance between two electrodes was set as 0.7 mm, and the diameter of the MRF sample was

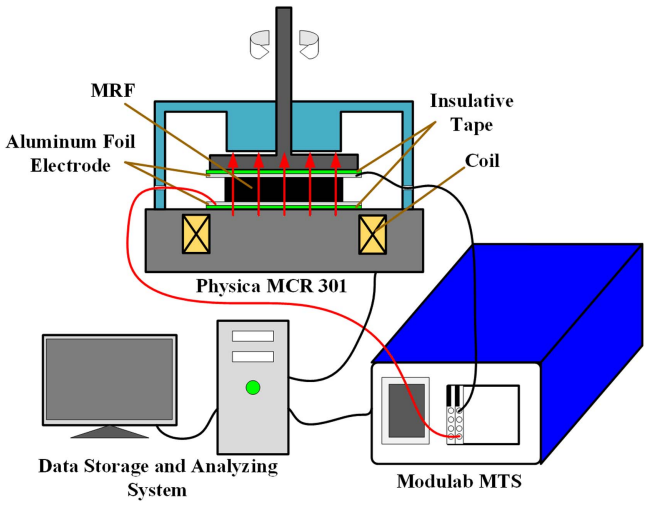

Figure 1. Schematic of the experiment system for the resistance measurements of MRFs.

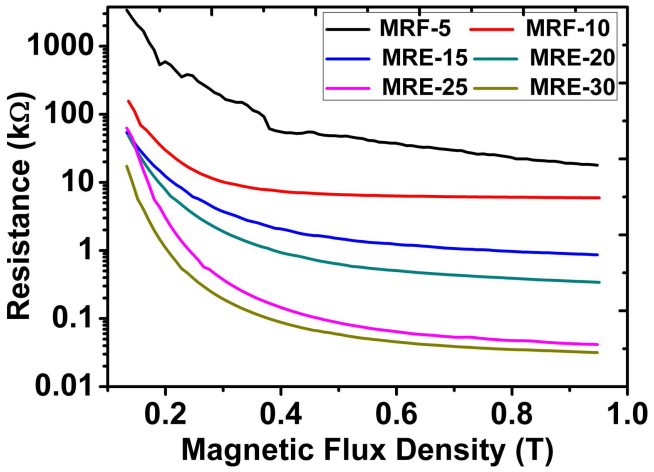

Figure 2. Resistance versus magnetic flux density of MRFs with different CIP contents.

20 mm. The oscillatory strain was set between 1% and 5%, and the oscillatory frequency was set between 0.05 and 0.1 Hz. The direct voltage was set to be 4 V. The resistance of the aluminum foil electrodes and the wire was less than 1 Ω, so it could be ignored in the experiments. During the test, the time of each measurement point was set as 1 s. All the measurements were implemented at 25 °C.

3. Results and discussion

3.1. Resistance of MRFs

When an external magnetic field was applied on the MRF, the conductive CIPs were aggregated to form chain or columnar-like micro-structures, thus the MRF sample transformed from non-conductive to conductive one. So, the influence of the magnetic field on the resistance of the MRF sample was firstly investigated. As shown in figure 2, with the increase of the magnetic field, the resistance of the MRF samples sharply decreased within 0.4 T and then tended to level off. When the magnetic field was small, though the CIPs were aggregated to form chain structures in the MRFs, the chains were short and could not contact with each other, and many internal gaps were presented in the chains [7], thus the conductivity of the MRF was poor. With the increase of the magnetic field, the short chains assembled into longer chains with a more compact microstructure which resulted in a higher conductivity. The aggregation of short chains is owing to lateral aggregation which occurs by a zippering mechanism [43–46]. So the conductivity of the MRFs was improved obviously. For example, when the magnetic field increased from 0.06 to 0.96 T, the resistance dropped from 63 kΩ to 42 Ω for MRF-25 and the conductivity increased about 1500 times. Under the same magnetic field, with the increase of CIP volume fraction, the resistance decreased sharply. When the CIP volume fraction increased, both the length and number of the chains increased. After a further rearrangement due to lateral aggregation, the columnar structures formed conducted to decrease sharply the resistance of the samples [45]. When the volume fraction increased from 5% to 30%, the resistance dropped from 18 kΩ to 32 Ω under a 0.96 T magnetic field, in which the conductivity increased about 560 times. To this end, the conductivity sharply increased with the increase of magnetic field and CIP volume fraction.

Then the influence of oscillatory shear on the resistance was investigated. As shown in figure 3, the larger strain led to the smaller resistance. For MRF-15, the resistance dropped from 597 to 311 Ω when the strain increased from 1% to 5%. With the increase of the frequency, the resistance slightly decreased. For MRF-15, the resistance dropped from 586 to 218 Ω when the frequency increased from 0.05 to 0.1 Hz. This phenomenon was the same for other samples except for MRF-5. When an oscillatory shear was applied on the MRF, the chain structures inside the MRF would oscillate together with the rotor of the rheometer. When the chains oscillated, they could touch each other allowing that the lateral aggregation to be more effective, as a result, longer, thicker and tighter columnar structures appeared. Therefore, a smaller resistance was obtained due to the tighter chain structures. When the strain was increased, the adjacent chains attached easier with each other to form columnar structures that led to a sharp decrease in the electrical resistance. At last, the conductivity of the samples could be greatly improved by the oscillatory shear [29, 45]. For MRF-5, the chain structures inside the sample were so scarce and short that the lateral aggregation and the microstructure rearrangement did not happen even when the strain was very large. Therefore, the oscillatory shear showed a tiny influence on the resistance for MRF-5.

Another interesting phenomenon obtained from figure 3 was that the resistance oscillated synchronously with the oscillatory shear. The average peak–peak amplitude of the resistance for each sample was obtained (table 2). The peak–peak value meant the difference between the maximum and the minimum of the resistance during one oscillation. For each sample, the larger the strain was, the larger the oscillatory peak–peak amplitude of the resistance was. For example, the amplitude of the resistance increased from 52 to 122 Ω for MRF-10 when the strain

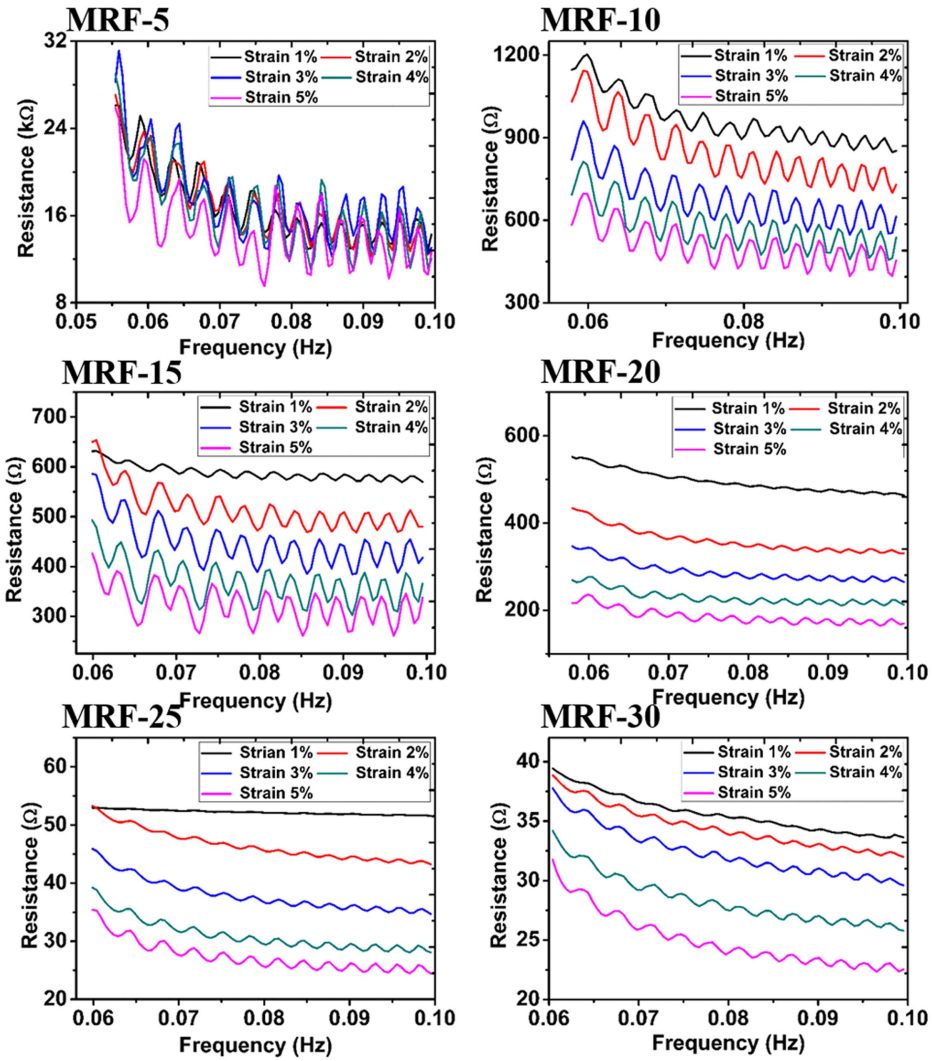

Figure 3. Resistance versus frequency for different samples and strain.

Table 2. Peak–peak amplitude of the resistance (Ω).

Sample	MRF-5	MRF-10	MRF-15	MRF-20	MRF-25	MRF-30
1%	2197	52	9	7	0.32	0.3
2%	3582	111	39	10	0.61	0.54
3%	3832	119	48	12	1.04	0.72
4%	5631	120	73	13	1.28	0.78
5%	6611	122	72	14	1.52	0.70

increased from 1% to 5%. When an oscillatory shear was applied, the chain structures would be stretched and the distance between the CIPs increased which resulted in the increasing of resistance. The peak–peak amplitude of the resistance decreased sharply with the increase of the CIP volume fraction. For example, while the strain is 3%, the amplitude of the resistance dropped from 3832 to 0.72 Ω when the CIP volume fraction increased from 5% to 30%. The chain structures in the MRFs with large CIP volume fraction were denser and thicker than those with smaller CIP volume fraction, so the influence of the oscillatory shear on the chain structures was small which would lead to a small oscillation of the resistance.

The time stability of the resistance was also investigated. Figure 4 showed the resistance versus time under static shear. Without the disturbance, the resistance kept almost constant, especially when the CIP volume fraction was large. This result indicated that the chain structures inside the MRF were stable when there was no disturbance applied on the samples. But for MRF-5, the resistance decreased with the increase of time. This was because that the isolated particles or small chains continued to aggregate with larger ones. The unstable structures were responsible for the decrease of the resistance.

Then, the resistance versus time under oscillatory shear was investigated (figure 5). Obviously, the resistance under

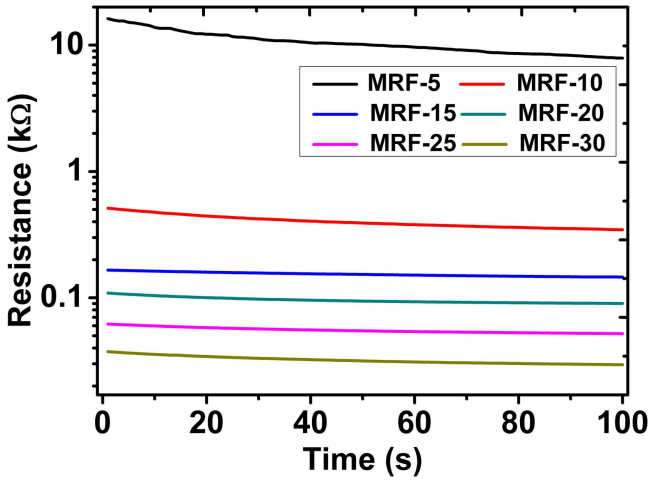

Figure 4. Resistance versus time under static condition and the magnetic flux density is 0.96 T.

oscillatory shear was smaller than the resistance under static condition. For MRF-15, the resistance decreased from 566 to 427 Ω when an oscillatory shear was applied. With increasing of the shear strain, the resistance decreased. For MRF-10, the resistance dropped from 1720 to 700 Ω when the strain increased from 1% to 5%. Under the oscillatory shear, the chain structure would contact with each other. The lateral aggregation and microstructure rearrangement happened, thus the chain structures inside the samples became tighter. In this case, more CIPs in the chains would contact with each other, thus the resistance decreased. In comparison to the resistance under static condition, the resistance under oscillatory shear decreased with the increase of time. Under the influence of oscillatory shear, the chain structures continually changed to an optimal state which led to the decrease of resistance [48]. The oscillation of the resistance also appeared in this test which was the same with that appeared in figure 3.

To sum up, without applying the external magnetic field, the CIPs were randomly dispersed resulted in a large resistance. As soon as an external magnetic field was applied, the CIPs began to assemble into chain structures and the resistance sharply decreased. When the magnetic field was small, the chain structures were short and had little chance to contact with each other. With increasing of the magnetic field, the short chain structures started assembling into longer ones through lateral aggregation and rearrangement. This reason would lead to the unceasingly decrease of the resistance and was responsible for the phenomenon shown in figure 2. When an oscillatory shear was applied on MRFs, the chain structures moved with the shear. They could contact with each other easier than the state under the static shear. For samples with large CIPs volume fraction, the chains structures inside MRFs were so long that they could easily contact with each other and assembled into longer ones. Then, the lateral aggregation and rearrangement appeared. When the stain amplitude increased, the moving range of chain structures was enlarged. So, the lateral aggregation and rearrangement intensified when the strain amplitude increased resulted in the decrease of resistance. But for samples with small CIPs volume fraction, the chain structures were so short that they could hardly contact with each other. The lateral aggregation and rearrangement could be ignored, thus the resistance of MRFs almost kept constantly when the strain amplitude increased (figure 3). Under a certain magnetic field and oscillatory shear, the structural rearrangement always existed and forwarded to optimal chain structures, thus the resistance slightly decreased with time (figures 4 and 5).

3.2. Theoretical model

In order to understand the conductive properties of MRFs, a particle–particle electrical resistance model based on dipole model was developed. In this section, the CIPs were assumed to have the same size and the CIP chains were formed like the necklace (figure 6(a)). The dark spheres represented the CIPs, the gray area represented the oil, and the light brown area represented the zone for the tunnel current. During the preparation of the MRFs, a layer of insulating film would be formed by the stearic acid which covered on the surface of CIPs. Since the resistance of the surface was far larger than that of CIPs, the resistance of MRFs mainly came from the interface resistance between the particles, named as tunnel resistance [49]. In this case, the resistance of the CIPs could be neglected contrasted with the tunnel resistance.

The conductivity J of tunnel current in the case of low voltage was given by [50]:

$$J = [3(2m\varphi)^{1/2}/2s](e/h)^2 V \times \exp[-(4\pi s/h)(2m\varphi)^{1/2}], \quad (1)$$

where m was the mass of electrons, e was the charge of electrons, φ was the height of the rectangular barrier, s was the particle distance, h was Planck's constant and V was the voltage across the film. Equation (1) gave the tunnel resistance between two planes, but between 2 spherical particles the separation was not constant. So equation (1) should be integrated between s_0 and d with a variable separation $s(r)$ where s_0 denoted the initial distance of two particles, d denoted the largest distance for the tunnel resistance. In our model, a was much smaller than r and the contact area of the tunnel resistance between two particles was assumed to be plane. Therefore, the tunnel resistance between two particles could be roughly estimated by using equation (1). The result was an approximation. J fell sharply with the increase of s. Therefore, we just focused on the tunnel current where the particle distance was less than d. When s was larger than d, the tunnel current disappeared. Equation (1) denotes the tunnel current between two adjacent particles. There are many particles in the volume unit and the series or parallel relationship between them is complex. So, another approximation is used to simulate the resistance of MRFs. We denoted the average resistivity of this area as ρ, then the resistance of the volume unit in figure 6(a) was expressed as:

$$R = \rho\frac{s}{A}, \quad (2)$$

where A was the area of the tunnel current and was expressed as:

$$A = \pi a^2 = \pi\left(r^2 - \left(r - \frac{h-s}{2}\right)^2\right) \approx \pi r(h-s). \quad (3)$$

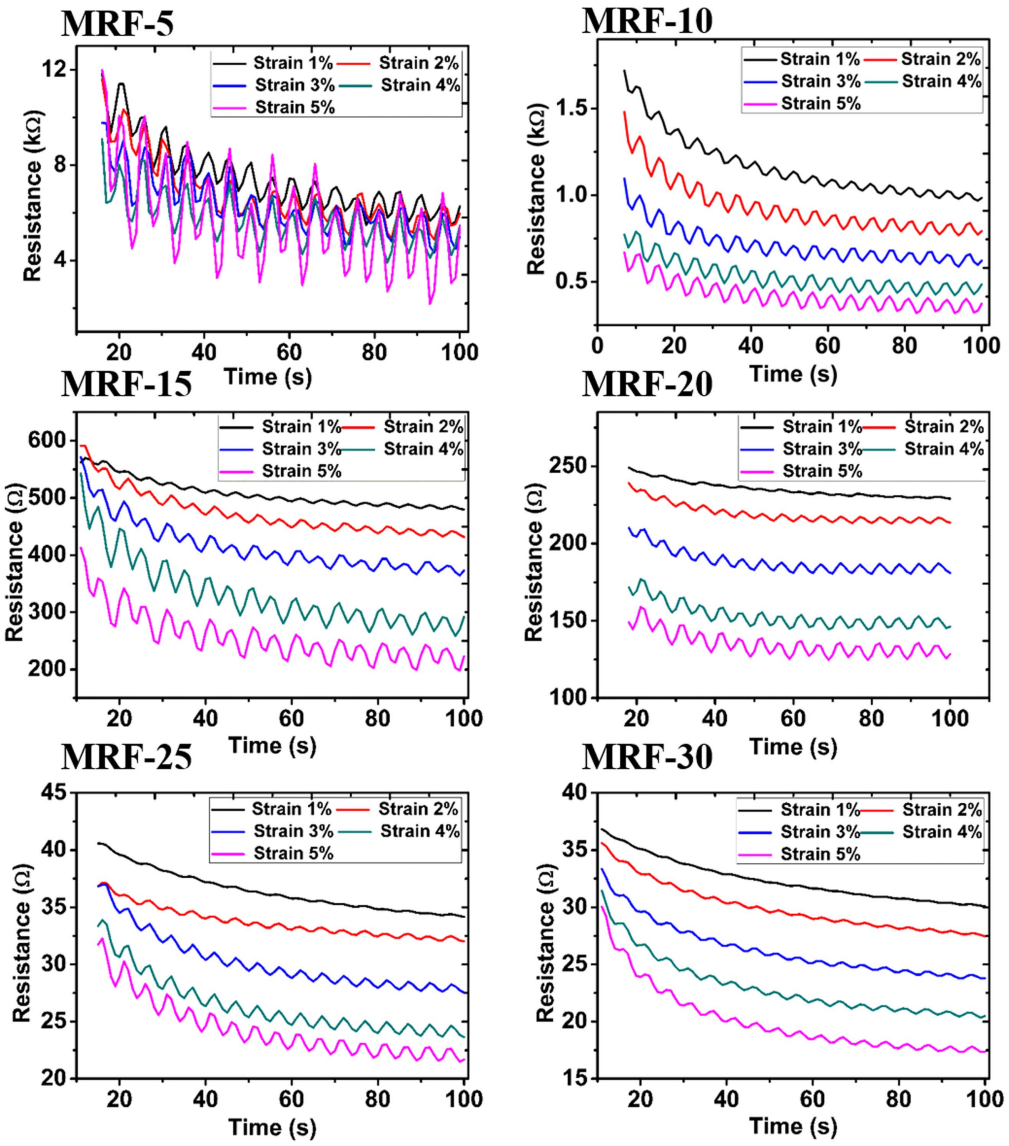

Figure 5. Resistance versus time under oscillatory shear, the frequency is 0.1 Hz and the magnetic flux density is 0.96 T.

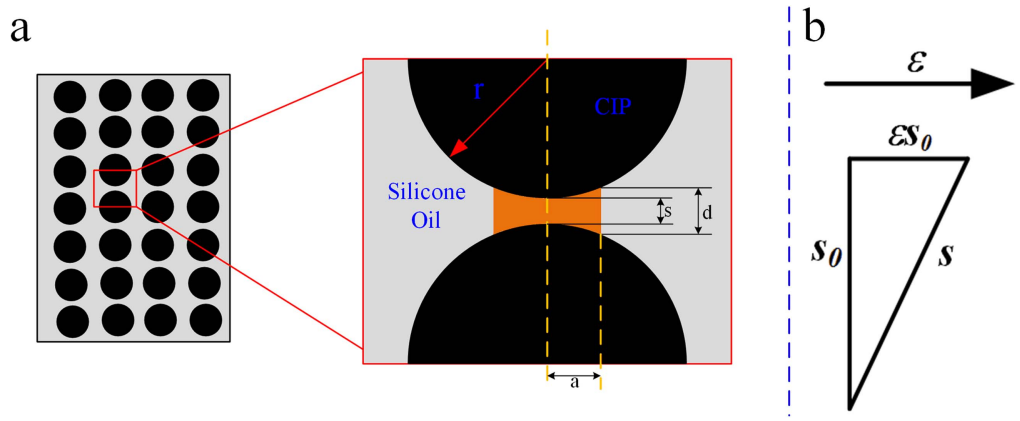

Figure 6. (a) Sketch of the particle–particle electrical resistance model. (b) Deformation of the distance when a shear is applied on the sample.

Here, s was much smaller than CIP radius r.

When a shear ε was applied on the MRF samples (figure 6(b)), the distance of the particles could be expressed as:

$$s = s_0\sqrt{1+\varepsilon^2} \approx s_0(1+|\varepsilon|). \quad (4)$$

Here, s_0 was the initial distance between the particles.

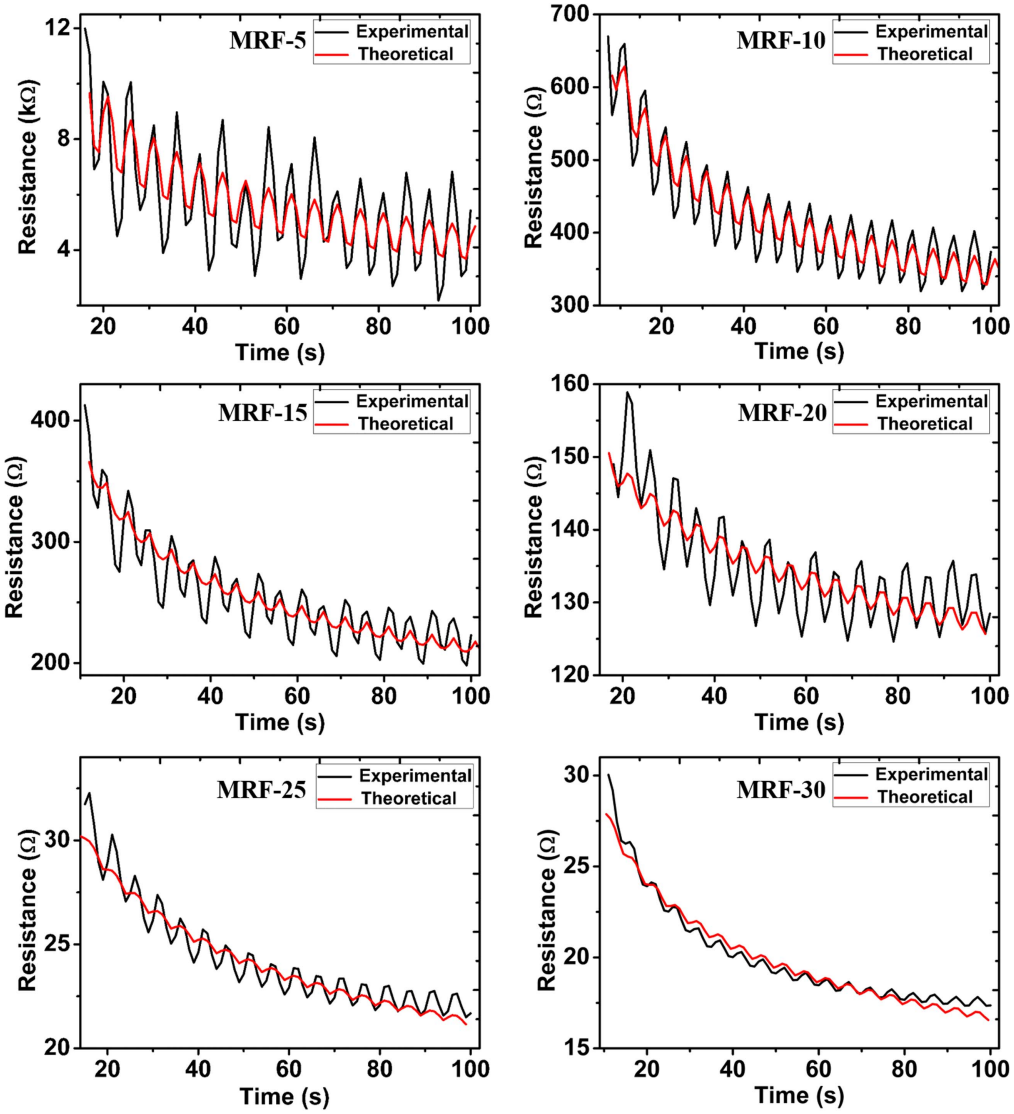

Figure 7. Comparison of the theoretical and experimental results of different samples. The shear amplitude is 5% and the frequency is 0.1 Hz.

Table 3. The relevant fitting parameters for different samples.

Parameters	ρ	$(d - s_0)/s_0$	c
MRF-5	2466.24	1.10	−0.42
MRF-10	155.22	1.06	−0.24
MRF-15	62.44	1.03	−0.25
MRF-20	51.23	0.99	−0.19
MRF-25	25.83	0.94	−0.19
MRF-30	18.98	0.91	−0.23

The oscillatory shear applied by the rheometer was sinusoidal and could be expressed as:

$$\varepsilon = \varepsilon_0 \cdot \sin(2\pi f \cdot t). \tag{5}$$

Here, ε_0 was the amplitude, f was the frequency of the oscillatory shear.

Finally, by using equations (2)–(5), we obtained:

$$\begin{aligned} R &= \rho \frac{s_0(1 + \varepsilon_0 |\sin(2\pi f \cdot t)|)}{\pi r(h - s_0(1 + \varepsilon_0 |\sin(2\pi f \cdot t)|))} \\ &= \rho \frac{1 + s_0 |\sin(2\pi f \cdot t)|}{\pi r\left(\frac{d - s_0}{s_0} - \varepsilon_0 |\sin(2\pi f \cdot t)|\right)}. \end{aligned} \tag{6}$$

Here, we obtained the expression of the resistance of the volume unit. Based on our assumption, the sectional area of the volume unit was given by:

$$A_1 = \frac{\frac{4}{3}\pi r^3}{\phi(2r + s)}. \tag{7}$$

Here, ϕ was the volume fraction of the sample.

The thickness of the sample was $Z = 0.7$ mm, the cross section area of the sample was $A = 314\,\text{mm}^2$. Thus the total

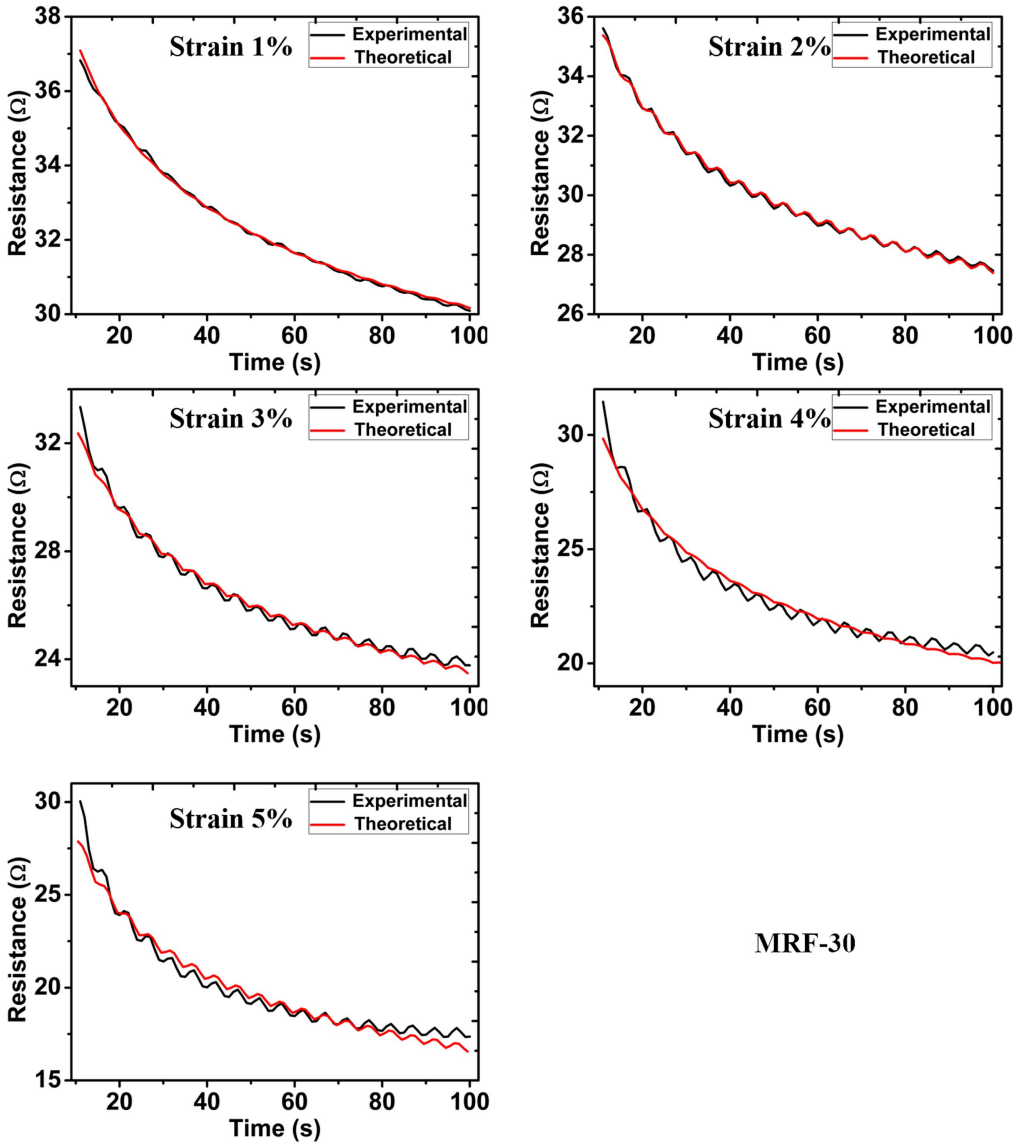

Figure 8. Comparison of theoretical and experimental results under different strain amplitude. The frequency is 0.1 Hz, the magnetic flux density is 0.96 T, the sample is MRF-30.

Table 4. The relevant fitting parameters for different strain amplitude.

Parameters	ρ	$(d-s_0)/s_0$	c
1%	18.72	1.00	−0.09
2%	18.64	0.99	−0.11
3%	17.98	0.98	−0.14
4%	17.91	0.98	−0.18
5%	18.98	0.98	−0.23

resistance of the samples could be expressed as:

$$R_\Sigma = R \cdot \frac{Z}{2r+s} \cdot \frac{A_1}{A} \approx \frac{\pi r Z}{3\phi A} \cdot R = \frac{\rho Z}{3\phi A} \cdot \frac{1+\varepsilon_0 \,|\sin(2\pi f t)|}{\frac{d-s_0}{s_0} - \varepsilon_0 \,|\sin(2\pi f t)|}. \quad (8)$$

Considering the influence of outside disturbances which mainly included the magnetic field, the oscillatory shear and the unavoidable vibration, a time factor c was added in equation (8) and was expressed as:

$$R_\Sigma = \frac{\rho Z}{3\phi A} \cdot \frac{1+\varepsilon_0 \,|\sin(2\pi f t)|}{\frac{d-s_0}{s_0} - \varepsilon_0 \,|\sin(2\pi f t)|} \cdot t^c. \quad (9)$$

3.3. Theoretical results and analysis

Figure 7 showed the comparison of theoretical and experimental results for different samples and the relevant fitting parameters were exhibited in table 3. Clearly, the theoretical results matched well with the experimental results. The relative initial particle distance ($(d-s_0)/s_0$) was almost equal to 1 with the increasing of the CIP volume fraction (table 3). Since the initial distance of two adjacent particles s_0 and the

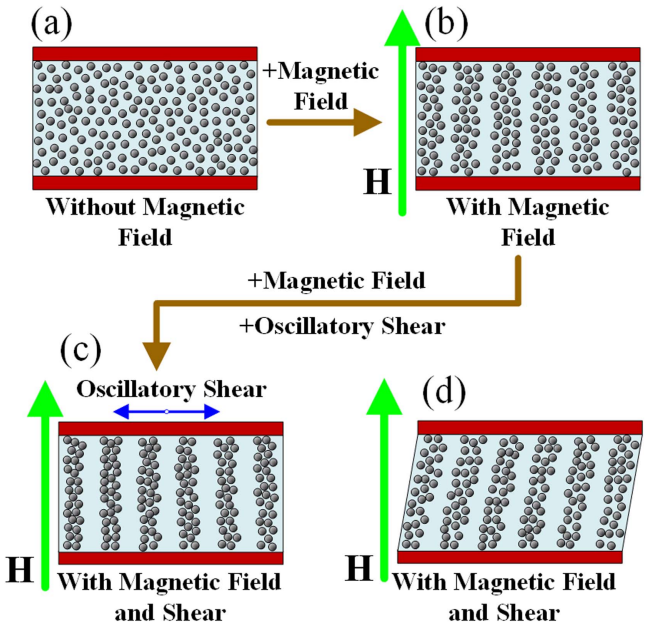

Figure 9. Schematic of the conductivity improving mechanism of the MRFs under a magnetic field and an oscillatory shear.

largest distance for the tunnel current d were constant and had nothing to do with the external testing conditions, so the relative initial particle distance $((d - s_0)/s_0)$ was almost the same for all experiments. The average resistivity (ρ) decreased from 2466.24 to 18.98 (Ω m) with the increase of the CIP volume fraction. As mentioned above, larger volume fraction meant more CIPs. In this case, more and longer chain structures would be formed. Therefore, the lateral aggregation and the rearrangement of the microstructure easily happened which resulted in a smaller average resistivity. For each sample, the time factor (c) fluctuated around -0.2, except for MRF-5. This indicated that the outside disturbance had the same influence on the MRFs with larger CIP volume fraction. During the tests, the rearrangement of the microstructure existed all the time [43–46] and the lateral aggregation was responsible for the decrease of the resistance. For MRF-5, the CIP numbers were so small that the chain structure was too thin, thus a very small disturbance could lead to collapse of the structures. So, the sample MRF-5 was more sensitive to time than other samples.

Figure 8 showed the comparison of the theoretical and experimental results for different strain amplitude and the relevant fitting parameters were obtained (table 4). It was found that the oscillatory shear almost hardly affected the relative initial particle distance $((d - s_0)/s_0)$ and the average resistivity (ρ). The initial particle distance s_0 and effective distance d were characteristic parameter for a certain sample, which were independent on the oscillatory shear. In this study, the s_0 and d were obtained by fitting the experimental data. Though the oscillatory shear caused sinusoidal changes of the chain structures inside MRF-30, the total influence of the strain on the structures was the same for different strain amplitudes. So, the relative initial particle distance $((d - s_0)/s_0)$ and the average resistivity (ρ) kept constantly for different strain amplitudes. The time factor (c) decreased with the increase of the strain amplitude. The larger strain amplitude presented a larger disturbance on the chains structure, so the long chain structures would be broken into short chains and the lateral aggregation and rearrangement was sharply. A longer time was needed for the MRF backing to the initial position which resulted in a larger time factor.

To further analyze the conductive characteristics of the MRFs, a possible mechanism was proposed (figure 9). Without the magnetic field, the CIPs randomly dispersed within the silicone oil. The gap between the CIPs was so large that there were only a few channels for the current flow (figure 9(a)), thus the conductivity was small. As soon as the external magnetic field was applied, the CIPs tended to aggregate closer to form chain structures because of the dipole force (figure 9(b)). Therefore, the conductivity of MRFs sharply increased when a magnetic field was applied. Though the chain structures were formed when an external magnetic field was applied, the chain structures were loose and the chains were small. So, the conductivity could be further improved. When an oscillatory shear was applied, the chains would contact with each other. The lateral aggregation and the rearrangement of the microstructure happened and tighter chain structures would be formed by the CIPs under the influence of magnetic field and oscillatory shear [45] (figure 9(c)). The microstructures would also realign under the influence of the oscillatory shear and the small chains would assemble into the main chains, the resistance decreased [44–47]. So, the conductivity of the MRF samples increased under the influence of oscillatory shear. Figure 9(d) exhibited the process of the oscillatory shear. The chain structures would be slightly stretched by the shear and the gap between the CIPs would increase which resulted in the increase of the resistance. So, the resistance decreased with the increasing of magnetic field and synchronously changed with the oscillatory shear [7, 29, 51].

4. Conclusion

In this work, the influence of oscillatory shear on the magnetic field dependent resistance of MRFs was researched. When a magnetic field was applied, chain structures would be formed which resulted in the decrease of the resistance. When the magnetic field increased from 0.06 to 0.96 T, the resistance dropped from 63 kΩ to 42 Ω for sample MRF-25 and the conductivity increased about 1500 times. The CIPs volume fraction could influence the numbers and density of the chain structures which exhibited a great influence on the conductivity of the MRFs. When the CIPs volume fraction increased from 5% to 30%, the resistance dropped from 18 kΩ to 32 Ω for 0.96 T magnetic field and conductivity increased about 565 times. When an oscillatory shear was applied on MRFs, the lateral aggregation and the rearrangement of the microstructure happened and tighter chain structures would be formed, so the conductivity of the samples could be greatly improved by the oscillatory shear. In samples with large CIP volume fraction, the chains were

longer and the number of chains was larger. So the occurrence of lateral aggregation and the rearrangement was easier when an oscillatory shear was applied. In samples with small CIP volume fraction, the chains were so short and the number of chains was so small that the lateral aggregation and the rearrangement could be ignored when an oscillatory shear was applied. So, the oscillatory shear had an obvious influence on the samples with large CIP volume fraction and few influenced on the samples with small CIP volume fraction. During the oscillatory shear, the chain structures would be continually stretched and recovered, which led to the oscillation of the resistance. The experimental results indicated that the average peak–peak amplitude of resistance decreased with the increase of the CIPs volume fraction and increased with strain. At last, a particle–particle model and a semi-empirical formula were proposed to investigate the resistance of the MRFs and the theoretical results matched well with the experimental results. This report would be benefit for the applications of MRFs in electrical and sensor fields.

Acknowledgments

Financial supports from the National Natural Science Foundation of China (Grant Nos. 11572309, 11572310), the Fundamental Research Funds for the Central Universities (WK2480000002), and the Strategic Priority Research Program of the Chinese Academy of Sciences (Grant No. XDB22040502) were gratefully acknowledged. This work was also supported by Collaborative Innovation Center of Suzhou Nano Science and Technology, and National Synchrotron Radiation Laboratory.

References

[1] Ashour O, Rogers C A and Kordonsky W 1996 Magnetorheological fluids: materials, characterization, and devices *J. Intell. Mater. Syst. Struct.* **7** 123–30
[2] Popplewell J and Rosensweig R 1996 Magnetorheological fluid composites *J. Phys. D: Appl. Phys.* **29** 2297
[3] Shilan S T, Mazlan S A, Ido Y, Hajalilou A, Jeyadevan B, Choi S B and Yunus N A 2016 A comparison of field-dependent rheological properties between spherical and plate-like carbonyl iron particles-based magneto-rheological fluids *Smart Mater. Struct.* **25** 095025
[4] Tang X, Zhang X, Tao R and Rong Y 2000 Structure-enhanced yield stress of magnetorheological fluids *J. Appl. Phys.* **87** 2634–8
[5] Jolly M R, Bender J W and Carlson J D 1999 Properties and applications of commercial magnetorheological fluids *J. Intell. Mater. Syst. Struct.* **10** 5–13
[6] Tang X, Zhang X and Tao R 2001 Enhance the yield shear stress of magnetorheological fluids *Int. J. Mod. Phys.* B **15** 549–56
[7] de Vicente J, Klingenberg D J and Hidalgo-Alvarez R 2011 Magnetorheological fluids: a review *Soft Matter* **7** 3701–10
[8] Li W, Chen G and Yeo S 1999 Viscoelastic properties of MR fluids *Smart Mater. Struct.* **8** 460–8
[9] Li W, Yao G, Chen G, Yeo S and Yap F 2000 Testing and steady state modeling of a linear MR damper under sinusoidal loading *Smart Mater. Struct.* **9** 95–102
[10] Gong X, Ruan X, Xuan S, Yan Q and Deng H 2014 Magnetorheological damper working in squeeze mode *Adv. Mech. Eng.* **6** 410158
[11] Li W and Du H 2003 Design and experimental evaluation of a magnetorheological brake *Int. J. Adv. Manuf. Technol.* **21** 508–15
[12] Liu B, Li W, Kosasih P and Zhang X 2006 Development of an MR-brake-based haptic device *Smart Mater. Struct.* **15** 1960–6
[13] Guo D, Hu H and Yi J 2004 Neural network control for a semi-active vehicle suspension with a magnetorheological damper *J. Vib. Control* **10** 461–71
[14] Lam A H-F and Liao W H 2003 Semi-active control of automotive suspension systems with magneto-rheological dampers *Int. J. Veh. Des.* **33** 50–75
[15] Arzanpour S and Golnaraghi F 2008 A novel semi-active magnetorheological bushing design for variable displacement engines *J. Intell. Mater. Syst. Struct.* **19** 989–1003
[16] Yao G, Yap F, Chen G, Li W and Yeo S 2002 MR damper and its application for semi-active control of vehicle suspension system *Mechatronics* **12** 963–73
[17] Nguyen Q H and Choi S B 2008 Optimal design of a vehicle magnetorheological damper considering the damping force and dynamic range *Smart Mater. Struct.* **18** 015013
[18] Erkus B, Abé M and Fujino Y 2002 Investigation of semi-active control for seismic protection of elevated highway bridges *Eng. Struct.* **24** 281–93
[19] Jung H J, Spencer B F Jr and Lee I W 2003 Control of seismically excited cable-stayed bridge employing magnetorheological fluid dampers *J. Struct. Eng.* **129** 873–83
[20] Li H, Liu M, Li J, Guan X and Ou J 2007 Vibration control of stay cables of the shandong binzhou yellow river highway bridge using magnetorheological fluid dampers *J. Bridge Eng.* **12** 401–9
[21] Udrea L E, Strachan N J, Vasile B and Rotariu O 2006 An *in vitro* study of magnetic particle targeting in small blood vessels *Phys. Med. Biol.* **51** 4869
[22] A Silva A, Silva E, Carrico A and T Egito E 2007 Magnetic carriers: a promising device for targeting drugs into the human body *Curr. Pharm. Des.* **13** 1179–85
[23] Hu W, Wang R, Lu Y and Pei Q 2014 An elastomeric transparent composite electrode based on copper nanowires and polyurethane *J. Mater. Chem.* C **2** 1298–305
[24] Sayyar S, Murray E, Thompson B, Chung J, Officer D L, Gambhir S, Spinks G M and Wallace G G 2015 Processable conducting graphene/chitosan hydrogels for tissue engineering *J. Mater. Chem.* B **3** 481–90
[25] Bica I 2010 Influence of the magnetic field on the electric conductivity of magnetorheological elastomers *J. Ind. Eng. Chem.* **16** 359–63
[26] Bica I, Anitas E M, Bunoiu M, Vatzulik B and Juganaru I 2014 Hybrid magnetorheological elastomer: influence of magnetic field and compression pressure on its electrical conductivity *J. Ind. Eng. Chem.* **20** 3994–9
[27] Bica I, Liu Y D and Choi H J 2012 Magnetic field intensity effect on plane electric capacitor characteristics and viscoelasticity of magnetorheological elastomer *Colloid Polym. Sci.* **290** 1115–22
[28] Martin J E, Anderson R A, Odinek J, Adolf D and Williamson J 2003 Controlling percolation in field-structured particle composites: observations of giant thermoresistance, piezoresistance, and chemoresistance *Phys. Rev.* B **67** 094207

[29] Pang H, Xuan S, Liu T and Gong X 2015 Magnetic field dependent electro-conductivity of the graphite doped magnetorheological plastomers *Soft Matter* **11** 6893–902
[30] Kchit N and Bossis G 2009 Electrical resistivity mechanism in magnetorheological elastomer *J. Phys. D: Appl. Phys.* **42** 105505
[31] Wang Y, Xuan S, Dong B, Xu F and Gong X 2015 Stimuli dependent impedance of conductive magnetorheological elastomers *Smart Mater. Struct.* **25** 025003
[32] Xu Y, Gong X, Liu T and Xuan S 2013 Magneto-induced microstructure characterization of magnetorheological plastomers using impedance spectroscopy *Soft Matter* **9** 7701–9
[33] Bica I 2009 Influence of the transverse magnetic field intensity upon the electric resistance of the magnetorheological elastomer containing graphite microparticles *Mater. Lett.* **63** 2230–2
[34] Kchit N, Lancon P and Bossis G 2009 Thermoresistance and giant magnetoresistance of magnetorheological elastomers *J. Phys. D: Appl. Phys.* **42** 105506
[35] Mietta J L, Ruiz M M, Antonel P S, Perez O E, Butera A, Jorge G and Negri R M 2012 Anisotropic magnetoresistance and piezoresistivity in structured Fe_3O_4–silver particles in PDMS elastomers at room temperature *Langmuir* **28** 6985–96
[36] Tian T, Li W, Alici G, Du H and Deng Y 2011 Microstructure and magnetorheology of graphite-based MR elastomers *Rheol. Acta* **50** 825–36
[37] Tian T, Li W and Deng Y 2011 Sensing capabilities of graphite based MR elastomers *Smart Mater. Struct.* **20** 025022
[38] Hsiao S T, Tien H W, Liao W H, Wang Y S, Li S M, Ma C C, Yu Y H and Chuang W-P 2014 A highly electrically conductive graphene–silver nanowire hybrid nanomaterial for transparent conductive films *J. Mater. Chem.* C **2** 7284–91
[39] Ribot J C, Guerrero-Sanchez C, Greaves T L, Kennedy D F, Hoogenboom R and Schubert U S 2012 Amphiphilic oligoether-based ionic liquids as functional materials for thermoresponsive ion gels with tunable properties via aqueous gelation *Soft Matter* **8** 1025–32
[40] Ribot J C, Guerrero-Sanchez C, Hoogenboom R and Schubert U S 2010 Thermoreversible ionogels with tunable properties via aqueous gelation of an amphiphilic quaternary ammonium oligoether-based ionic liquid *J. Mater. Chem.* **20** 8279–84
[41] Ribot J C, Guerrero Sanchez C, Hoogenboom R and Schubert U S 2010 Aqueous gelation of ionic liquids: reverse thermoresponsive ion gels *Chem. Commun.* **46** 6971–3
[42] Guerrero Sanchez C, Lara Ceniceros T, Jimenez Regalado E, Raşa M and Schubert U S 2007 Magnetorheological fluids based on ionic liquids *Adv. Mater.* **19** 1740–7
[43] Cutillas S, Bossis G and Cebers A 1998 Rheological properties of MR fluids *Phys. Rev.* E **57** 804–11
[44] Laskar J M, Philip J and Raj B 2009 Experimental evidence for reversible zippering of chains in magnetic nanofluids under external magnetic fields *Phys. Rev.* E **80** 041401
[45] Moctezuma R E, Donado F and Arauz-Lara J L 2013 Lateral aggregation induced by magnetic perturbations in a magnetorheological fluid based on non-Brownian particles *Phys. Rev.* E **88** 032305
[46] Moctezuma R E, Arauz-Lara J L and Donado F 2014 Multifractality in dilute magnetorheological fluids under an oscillating magnetic field *Phys. Rev.* E **90** 062303
[47] Buongiorno J, Venerus D C and Prabhat N 2009 A benchmark study on the thermal conductivity of nanofluids *J. Appl. Phys.* **106** 094312
[48] Celzard A, Marêché J, Payot F and Furdin G 2002 Electrical conductivity of carbonaceous powders *Carbon* **40** 2801–15
[49] Kogut L and Komvopoulos K 2003 Electrical contact resistance theory for conductive rough surfaces *J. Appl. Phys.* **94** 3153–62
[50] Simmons J G 1963 Electric tunnel effect between dissimilar electrodes separated by a thin insulating film *J. Appl. Phys.* **34** 2581–90
[51] Bica I 2006 The influence of the magnetic field on the electrical magnetoresistance of magnetorheological suspensions *J. Magn. Magn. Mater.* **299** 412–8